

Analytical derivation and expansion of the anti-Kibble–Zurek scaling in the transverse field Ising model

Kaito Iwamura¹ and Takayuki Suzuki²

¹*Department of Physics, Waseda University, Tokyo 169-8555, Japan*

²*National Institute of Information and Communications Technology, Nukui-Kitamachi 4-2-1, Koganei, Tokyo 184-8795, Japan*

A defect density which quantifies the deviation from the spin ground state characterizes non-equilibrium dynamics during phase transitions. The widely recognized Kibble-Zurek scaling predicts how the defect density evolves during phase transitions. However, it can be perturbed by noise, leading to anti-Kibble-Zurek scaling. In this research, we analytically investigate the effect of Gaussian white noise on the transition probabilities of the Landau-Zener model. We apply this model to the one-dimensional transverse field Ising model and derive an analytical approximation for the defect density. Our analysis reveals that under small noise conditions, the model follows an anti-Kibble-Zurek scaling. As the noise increases, a new scaling behavior emerges, showing higher accuracy than previously reported. Furthermore, we identify the parameters that optimize the defect density based on the new scaling. This allows for the refinement of optimized parameters with greater precision and provides further validations of previously established scaling.

I. INTRODUCTION

In modern quantum physics, understanding the dynamics of phase transitions is essential for quantum information and quantum technology. Notably, the Quantum Kibble–Zurek mechanism (QKZM) has attracted considerable attention [1–4]. QKZM serves as a theoretical framework that provides scaling laws for quantum phase transitions in the adiabatic limit. QKZM is an application of the Kibble–Zurek mechanism to quantum systems, which was originally proposed within cosmology [5, 6] and later applied to condensed matter systems [7–9].

The transverse field XY-chain model and the transverse field Ising model are systems where the spins are excited by an external magnetic field. The QKZM suggests that quantum phase transitions follow particular scaling laws in the adiabatic regime [1–4, 10]. It allows us to predict the defect density, which represents deviations from the ground state.

In the context of quantum control, it is desirable to minimize defects. According to the QKZM law, as the driving speed v decreases, the number of defects decreases as well. The limit as v approaches zero is referred to as the adiabatic limit. However, recent study have observed an interesting phenomenon called the anti-Kibble–Zurek mechanism (anti-KZM) [11–15], where the scaling breaks down in the adiabatic region when external noise is introduced into the system. Anti-KZM may be effective in some experiments deriving scaling with the transverse Ising chain [16–20] or with other systems [21–27]. The scaling law proposed by anti-KZM argues that defects become larger when the driving speed v is small, contrary to the QKZM. This suggests that there exists a specific non-zero optimized driving speed, denoted by v_{opt} , which minimizes defects. Therefore, clarifying the scaling based on anti-KZM is important and it is necessary to conduct theoretical research.

In previous research simulating the defect density in the transverse field XY-chain model with a Gaussian white noise [12], the Hamiltonian has been considered

$$\begin{aligned} H_{XY}(t) &= - \sum_{j=1}^N (J_x \sigma_j^x \sigma_{j+1}^x + J_y \sigma_j^y \sigma_{j+1}^y + h \sigma_j^z), \\ &= - \frac{K}{2} \sum_{j=1}^N ((1 + \phi) \sigma_j^x \sigma_{j+1}^x + (1 - \phi) \sigma_j^y \sigma_{j+1}^y) - h \sum_{j=1}^N \sigma_j^z. \end{aligned}$$

Here, $K = J_x + J_y$, $\phi = \frac{J_x - J_y}{K}$. The number of spins N is assumed to be sufficiently large, implying a thermodynamic limit. The parameter t takes from an infinite past to an infinite future. The system evolves from the initial state, which is the ground state. At the final time, the defect density which is the deviation from the ground state is calculated numerically. The time-dependence is introduced through either $h(t) = vt + \gamma(t)$, $J_x(t) = vt + \gamma(t)$, or $\phi(t) = vt + \gamma(t)$. Here, v is the driving speed, and $\gamma(t)$ denotes Gaussian noise with zero mean and the second moment that satisfies $\gamma(t) = 0$, $\overline{\gamma(t)\gamma(t')} = W^2 \delta(t - t')$. The scaling of the defect density n for small W is represented as [12]

$$n \sim cv^\beta + rv^{-1}. \quad (1)$$

Here, c , r , and β are coefficients determined by the choice of the system and the parameters. The first term represents the well-known term identified in QKZM, while the second term which is proper to v^{-1} emerges due to the introduction of noise. The mechanism is referred to as anti-KZM, where n increases as v decreases. This is a numerically established result and are not analytically demonstrated.

The defect density is derived by transforming the system into a time-dependent quantum two-level system through the Jordan–Wigner transformation. Models

such as the one-dimensional transverse field XY-chain model and the one-dimensional transverse field Ising model, which incorporate noise, are transformed into noise-induced Landau–Zener models. When introducing the Gaussian white noise $\gamma(t)$, it is established that the density matrix follows a master equation [13, 28, 29]. The density matrix derives the transition probability and the defect density.

In a numerical research on the noise-induced transverse field Ising model with Gaussian white noise [13], corresponding to the case of $J_x(t) = vt + \gamma(t)$, $J_y = 0$, $h(t) = J - vt - \gamma(t)$, $t \in [0, J/v]$, the similar anti-KZM scaling as in Eq. (1) has been confirmed. Unfortunately, the scaling of v^{-1} in Eq. (1) leads to divergence for small v . However, as stated in [13], applying the Kayanuma formula [30] provides an asymptotic expression in the small v regime

$$n^{\text{Kayanuma}} \sim \frac{1}{2} - \frac{\sqrt{v}}{4\pi J},$$

which does not diverge. This formula is derived under the approximation that the noise is sufficiently large. This result converges asymptotically to $1/2$ as v approaches zero, which is consistent with the numerical simulation. However, in the other region this formula is not valid. Therefore, for small v , a more precise approximate solution is required.

The analytical derivation of the transition probability in the noise-induced Landau–Zener model has been done in previous studies [30, 31]. However, the noise considered in these analyses is a different types of noise, expressed as $\tilde{\gamma}(t)$. Here, $\tilde{\gamma}(t)$ represents Gaussian noise with $\overline{\tilde{\gamma}(t)} = 0$ and $\overline{\tilde{\gamma}(t)\tilde{\gamma}(t')} = W^2 e^{-\Gamma|t-t'|}$. It may not be feasible to directly apply Gaussian white noise to derive these approximate solutions. This is because the study [30] assumes a large noise in the last and the system considered in [31] does not cover all cases. The research [14] analytically derives the defect density introduced the noise $\tilde{\gamma}(t)$ in the nearest-neighbor interaction term by using the result from [31]. In addition, the work [15] has established anti-KZM scaling in fully connected models. Other studies have explored systems under various perturbations, such as a recycling term [32, 33], a time-dependent simple harmonic oscillator [34–37], and a dissipative thermal bath [38–44].

This research aims to analytically derive the defect density and to reproduce the anti-KZM in the one-dimensional transverse field Ising model with Gaussian white noise in the transverse field term. In addition, we derive a more precise scaling than the previously proposed anti-KZM scaling in previously unexplored regions. To this end, we first perform an analytical derivation of the transition probabilities from the ground state in the Landau–Zener model with Gaussian white noise. Second, by applying approximate solutions of the Landau–Zener model to the transverse field Ising model, we find the anti-KZM scaling. Finally, we examine the correlation between the optimized driving speed v_{opt} with respect

to the parameter W^2 , which represents the magnitude of the noise. While the scaling of v_{opt} with W^2 is already known to be $v_{\text{opt}} \propto W^{\frac{4}{3}}$ in the small W^2 regime from numerical calculations [12, 13], our research extends this analysis to the unexplored regime of large W^2 .

In Sec. II, we calculate the transition probability of the Landau–Zener model with Gaussian white noise. In Sec. III, we apply the formula discussed in Sec. II to the transverse field Ising chain with Gaussian white noise in the adiabatic limit to determine the scaling of the defect density. Section IV is dedicated to a discussion on the parameters that minimize the defect density. Section V is the conclusion.

II. THE LANDAU–ZENER MODEL WITH GAUSSIAN WHITE NOISE

In the natural units, consider the following two-level Hamiltonian system

$$H_{\text{LZ+noise}}(t) = H_0(t) + H_{\text{noise}}(t), \quad (2)$$

$$H_0(t) = \frac{vt}{2}\sigma^z + J\sigma^x, \quad H_{\text{noise}}(t) = \gamma(t)\sigma^z.$$

Here, $\gamma(t)$ represents Gaussian white noise satisfying $\overline{\gamma(t)} = 0$ and $\overline{\gamma(t)\gamma(t')} = W^2\delta(t-t')$, where W^2 and J are constants with an energy dimension. The quantities with an overline indicate that they are ensemble-averaged. The driving speed v has dimensions of the square of the energy. The term $H_0(t)$ corresponds to a Landau–Zener-type Hamiltonian. It has already been well analyzed, and the time-evolution operator is obtained with the parabolic cylinder functions.

The expectation value of a time-independent and noise-independent observable P at an arbitrary time t can be expressed as

$$\langle \overline{P(t)} \rangle = \text{Tr} \left[\overline{\rho(t)} P \right] = \text{Tr} \left[\overline{U(t, t_i) \rho(t_i) U^\dagger(t, t_i) P} \right], \quad (3)$$

where the density matrix $\rho(t)$ and the time-evolution operator $U(t, t_i)$ include contributions of noise. t_i is an initial time and $U(t_i, t_i) = 1$. The noise-averaged density matrix $\overline{\rho(t)}$ follows the master equation

$$\frac{d}{dt} \overline{\rho(t)} = -i \left[H_0(t), \overline{\rho(t)} \right] + \frac{1}{2} W^2 \left[\left[\sigma^z, \overline{\rho(t)} \right], \sigma^z \right].$$

This equation is verified in [13] by Novikov’s theorem [45] and by the other derivations [28, 29]. Employing the dimensionless parameters: the time parameter $\tau = \sqrt{v}t$, the adiabatic parameter $\kappa = J^2/v$, and the noise strength parameter $\lambda = W^2/J$, the master equation is expressed as

$$\begin{aligned} \frac{d}{d\tau} \overline{\rho(\tau)} &= -i \left[H_0(\tau), \overline{\rho(\tau)} \right] + \frac{\lambda}{2} \sqrt{\kappa} \left[\left[\sigma^z, \overline{\rho(\tau)} \right], \sigma^z \right], \\ H_0(\tau) &= \frac{\tau}{2} \sigma^z + \sqrt{\kappa} \sigma^x. \end{aligned} \quad (4)$$

At an initial time τ_i chosen to be the infinite past, we set the initial condition as the ground state $\rho(\tau_i) = |\uparrow\rangle\langle\uparrow|$. Here, $\sigma_z|\uparrow\rangle = |\uparrow\rangle$. To determine the probability of maintaining $|\uparrow\rangle\langle\uparrow|$, which corresponds to the transition probability, we define $P = |\uparrow\rangle\langle\uparrow|$ in Eq. (3). We solve the time evolution equation for $\rho(\tau)$ up to the final time τ_f by the master equation Eq. (4) and calculate the transition probability $\langle\overline{P(\tau_f)}\rangle$. The first term on the right-hand side of Eq. (4) represents the unitary term. If only this term is considered, analytical solutions for the density matrix $\rho(\tau)$ at any time are obtained with the parabolic cylinder functions. It is known that $\langle\overline{P(\tau_f)}\rangle = e^{-2\pi\kappa}$. As the parameter κ increases, the transition probability decreases. The second term in Eq. (4), the dissipation term, accounts for the interaction with noise. The presence of this term leads to an increase in the transition probability as κ increases. The master equation Eq. (4) exhibits explicit time dependence solely through H_0 . If the initial time is the infinite past and the final time is the infinite future, the shift of the time τ of H_0 does not depend on the transition probability at the final time.

In this study, we consider the case where the noise is sufficiently small, i.e., $\lambda \ll 1$. We divide κ into three distinct regions: (i) the small region ($\kappa \ll 1$), (ii) the medium region ($1 \ll \kappa \ll \frac{1}{\lambda}$), and (iii) the large region ($\frac{1}{\lambda} \ll \kappa$). In the regions (i) and (ii), we employ perturbation approximation up to the first order with respect to λ in Sec. II A. On the other hand, in the regions (ii) and (iii), we employ the adiabatic approximation in Sec. II B. By connecting the approximations, we derive the globally effective approximation in Sec. II C.

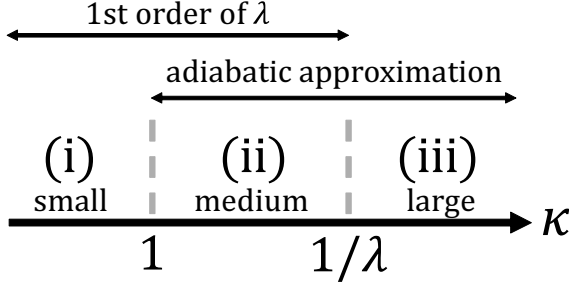


FIG. 1. A schematic diagram illustrating the domains of κ : (i), (ii), and (iii). Over each region, the corresponding approximation methods are indicated.

A. First-order perturbation for noise

In this subsection, we consider (i) the small region ($\kappa \ll 1$) and (ii) the medium region ($1 \ll \kappa \ll 1/\lambda$). In these regions, we analytically approximate the solution up to the first order with respect to λ .

The Hamiltonian $H_0(\tau)$ is referred to as the Landau-Zener model, and the time-evolution operator for $H_0(\tau)$ is expressed as

$$U_0(\tau, \tau_i) = \begin{pmatrix} f(\tau, \tau_i) & -g^*(\tau, \tau_i) \\ g(\tau, \tau_i) & f^*(\tau, \tau_i) \end{pmatrix}, \quad (5)$$

$$f(\tau, \tau_i) = e^{-\pi\kappa/2} D_{i\kappa}(e^{-\frac{\pi}{4}i\tau_i}) D_{-i\kappa}(e^{\frac{\pi}{4}i\tau}) + e^{-\pi\kappa/2} \sqrt{\kappa} D_{-i\kappa-1}(e^{\frac{\pi}{4}i\tau_i}) \sqrt{\kappa} D_{i\kappa-1}(e^{-\frac{\pi}{4}i\tau}),$$

$$g(\tau, \tau_i) = e^{-\pi\kappa/2} e^{\frac{\pi}{4}i} D_{i\kappa}(e^{-\frac{\pi}{4}i\tau_i}) \sqrt{\kappa} D_{-i\kappa-1}(e^{\frac{\pi}{4}i\tau}) - e^{-\pi\kappa/2} e^{\frac{\pi}{4}i} \sqrt{\kappa} D_{-i\kappa-1}(e^{\frac{\pi}{4}i\tau_i}) D_{i\kappa}(e^{-\frac{\pi}{4}i\tau}).$$

We set the initial condition as $U(\tau_i, \tau_i) = 1$. Moving to the interaction picture

$$\tilde{\rho}(\tau) = U_0^\dagger(\tau, \tau_i) \rho(\tau) U_0(\tau, \tau_i),$$

$$\tilde{\sigma}_z(\tau, \tau_i) = U_0^\dagger(\tau, \tau_i) \sigma_z U_0(\tau, \tau_i),$$

the transition probability $\langle\overline{P(\tau)}\rangle$ and the time-evolution equation for $\tilde{\rho}(\tau)$ are given by

$$\langle\overline{P(\tau)}\rangle = \text{Tr} \left[U_0(\tau, \tau_i) \tilde{\rho}(\tau) U_0^\dagger(\tau, \tau_i) P \right],$$

$$\frac{d}{d\tau} \tilde{\rho}(\tau) = \frac{1}{2} \lambda \sqrt{\kappa} \left[\tilde{\sigma}_z(\tau, \tau_i), \left[\tilde{\rho}(\tau), \tilde{\sigma}_z(\tau, \tau_i) \right] \right]. \quad (6)$$

By integrating Eq. (6) with respect to τ , the transition probability up to the first order in λ is given by

$$\langle\overline{P(\tau_f)}\rangle = \langle\uparrow| U_0(\tau_f, \tau_i) \tilde{\rho}(\tau_f) U_0^\dagger(\tau_f, \tau_i) |\uparrow\rangle$$

$$= \langle\uparrow| U_0(\tau_f, \tau_i) \rho(\tau_i) U_0^\dagger(\tau_f, \tau_i) |\uparrow\rangle + \int_{\tau_i}^{\tau_f} d\tau \langle\uparrow| U_0(\tau_f, \tau_i) \frac{\lambda \sqrt{\kappa}}{2} [\tilde{\sigma}_z(\tau, \tau_i), [\rho(\tau_i), \tilde{\sigma}_z(\tau, \tau_i)]] U_0^\dagger(\tau_f, \tau_i) |\uparrow\rangle + \mathcal{O}(\lambda^2).$$

Substituting the specific form of U_0 and taking the limits as $\tau_i \rightarrow -\infty$ and $\tau_f \rightarrow \infty$, the expression can be represented

as

$$\langle \overline{P(\tau_f)} \rangle = e^{-2\pi\kappa} + 4\lambda\sqrt{\kappa} \int_{-\infty}^{\infty} d\tau \left(|X(\tau)|^2 + \frac{2e^{-2\pi\kappa}}{1 - e^{-2\pi\kappa}} (\text{Re}(X(\tau)))^2 + \frac{2e^{-\pi\kappa}}{1 - e^{-2\pi\kappa}} \text{Re}(X(\tau))Y(\tau) \right) + \mathcal{O}(\lambda^2), \quad (7)$$

$$X(\tau) = \kappa e^{-\frac{\pi\kappa}{2}} D_{-i\kappa-1}(e^{\frac{i\pi}{4}}\tau) D_{i\kappa-1}(-e^{-\frac{i\pi}{4}}\tau),$$

$$Y(\tau) = \frac{\kappa}{2} e^{-\frac{\pi\kappa}{2}} \left(|D_{-i\kappa-1}(e^{\frac{i\pi}{4}}\tau)|^2 + |D_{i\kappa-1}(-e^{-\frac{i\pi}{4}}\tau)|^2 \right).$$

The formulas used in the derivation are given in Appendix A. Both $|X(\tau)|$ and $|Y(\tau)|$ do not exceed 1. We derive $\overline{\rho(\tau)}$ by evolving using Eq. (6) from the initial time τ_i , and obtain $\langle \overline{P(\tau_f)} \rangle$, which includes contributions up to the infinite order of λ . Eq. (6) does not have an analytical solution and is therefore computed numerically. On the other hand, the approximate solution up to the first order of λ is derived by calculating Eq. (7). While the analytical solutions for transition probability at arbitrary times are not derived, this subsection focuses on deriving an approximate solution at the final time. These two numerical plots are illustrated in Fig. 2. According to Fig. 2, the transition probability approaches the results of numerical simulations and first-order approximations when κ is small. As κ increases beyond this point, the accuracy of the approximation deteriorates due to the failure of the condition $\lambda\kappa \ll 1$.

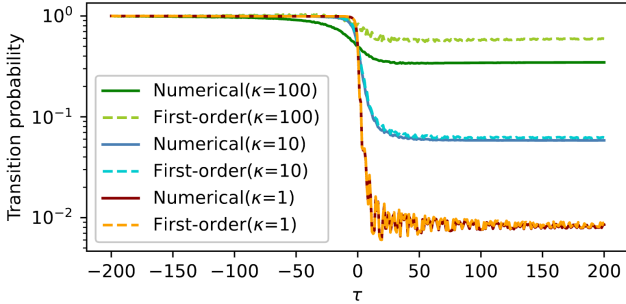


FIG. 2. Comparison between numerical results obtained from solving the time evolution through the master equation Eq. (6) and the first-order approximation of λ Eq. (7). The solid lines (Numerical) represent the numerical results. The dashed lines (first order) represent the first-order approximation. Both simulations cover a time interval from $\tau_i = -200$ to $\tau_f = 200$, with λ set to 10^{-3} and κ set to 100, 10, and 1.

We seek the approximate solution for Eq. (7) in the regions (i) and (ii). First, we begin the region (i): small κ . When $\kappa = 0$, both $X(\tau)$ and $Y(\tau)$ equal zero, leading to the dominance of the first term of the right-hand side in Eq. (7). Consequently, we can approximate the expression as

$$\langle \overline{P(\tau_f)} \rangle \stackrel{(i)}{\sim} e^{-2\pi\kappa}.$$

This is strongly suppressed where $\kappa \gg 1$, and it only holds significance in regions where κ is small.

Second, consider the region (ii): medium κ . Given the condition $\kappa \gg 1$, dropping terms proportional to $e^{-\pi\kappa}$ is an effective approximation. Under this approximation, only the term with $|X(\tau)|^2$ in Eq. (7) contributes. Thus, the transition probability at the final time can be approximated as

$$\langle \overline{P(\tau_f)} \rangle \sim 4\lambda\sqrt{\kappa} e^{-\pi\kappa} \kappa^2 \times \int_{-\infty}^{\infty} d\tau \left| D_{-i\kappa-1}(e^{\frac{i\pi}{4}}\tau) D_{-i\kappa-1}(-e^{\frac{i\pi}{4}}\tau) \right|^2.$$

Ignoring the term of $\mathcal{O}(\kappa^{-2})$ and $\mathcal{O}(e^{-\pi\kappa})$, $\langle \overline{P(\tau_f)} \rangle$ is approximated as

$$\langle \overline{P(\tau_f)} \rangle \stackrel{(ii)}{\sim} 2\pi\lambda\kappa. \quad (8)$$

The detailed derivation is conducted in Appendix B and C. It is evident that Eq. (8) becomes zero when $\kappa = 0$.

Therefore, effective solutions in the region where κ is small are dominant only within the region, and conversely, effective solutions in the region where κ is large are dominant only within the region. Hence, the transition probability in both regions (i) and (ii) can be approximated as the sum of effective solutions,

$$\langle \overline{P(\tau_f)} \rangle \stackrel{(i),(ii)}{\sim} e^{-2\pi\kappa} + 2\pi\lambda\kappa. \quad (9)$$

The first term on the right-hand side represents the transition probability of the Landau-Zener model in the absence of noise. The second term corresponds to the influence of the noise. Despite being a transition probability, the right-hand side diverges as $\kappa \rightarrow \infty$ due to the noise effect. This approximate solution is valid only in the region where $\lambda\kappa \ll 1$, and it is not allowed to take the limit of κ approaching infinity. This is confirmed by the comparison between numerical and approximate solutions in Fig. 2. As κ increases, the influence of higher-order contributions of λ becomes significant, leading to a deterioration in the accuracy of the first-order approximation.

B. Adiabatic approximation

In the regions (ii) and (iii), that is $\kappa \gg 1$, the adiabatic approximation is employed as [33]. The equations of the components of the density matrix $\overline{\rho(\tau)}$, derived from the master equation Eq. (4), are

$$\overline{\rho(\tau)} = \begin{pmatrix} \rho_{11}(\tau) & \rho_{12}(\tau) \\ \rho_{21}(\tau) & \rho_{22}(\tau) \end{pmatrix},$$

$$\begin{aligned} \frac{d}{d\tau} |\rho(\tau)\rangle\rangle &= \frac{d}{d\tau} (\rho_{11}(\tau) \ \rho_{12}(\tau) \ \rho_{21}(\tau) \ \rho_{22}(\tau))^T \\ &= \begin{pmatrix} 0 & i\sqrt{\kappa} & -i\sqrt{\kappa} & 0 \\ i\sqrt{\kappa} & -i\frac{\tau}{2} - \lambda\sqrt{\kappa} & 0 & -i\sqrt{\kappa} \\ -i\sqrt{\kappa} & 0 & i\frac{\tau}{2} - \lambda\sqrt{\kappa} & i\sqrt{\kappa} \\ 0 & -i\sqrt{\kappa} & i\sqrt{\kappa} & 0 \end{pmatrix} \begin{pmatrix} \rho_{11}(\tau) \\ \rho_{12}(\tau) \\ \rho_{21}(\tau) \\ \rho_{22}(\tau) \end{pmatrix}. \end{aligned}$$

The term $\mathcal{O}(\lambda^2)$ is neglected in the following analysis in this subsection. Let $z(\tau) = \frac{\tau}{4\sqrt{\kappa}}$. The time evolution with this Liouvillian is calculated by using the adiabatic approximation [46]. The specific calculations are detailed in Appendix D. The eigenvalues of the Liouvillian are

$$\begin{aligned} \chi_1(\tau) &= 0, \\ \chi_2(\tau) &= -\frac{\lambda}{z^2(\tau) + 1} \sqrt{\kappa}, \\ \chi_3(\tau) &= -\frac{2z^2(\tau) + 1}{2z^2(\tau) + 2} \lambda\sqrt{\kappa} - 2i\sqrt{z^2(\tau) + 1}\sqrt{\kappa}, \\ \chi_4(\tau) &= -\frac{2z^2(\tau) + 1}{2z^2(\tau) + 2} \lambda\sqrt{\kappa} + 2i\sqrt{z^2(\tau) + 1}\sqrt{\kappa}. \end{aligned}$$

The Liouvillian is diagonalized with 4×4 matrix $S(\tau)$ as

$$S(\tau) \begin{pmatrix} \chi_1(\tau) & 0 & 0 & 0 \\ 0 & \chi_2(\tau) & 0 & 0 \\ 0 & 0 & \chi_3(\tau) & 0 \\ 0 & 0 & 0 & \chi_4(\tau) \end{pmatrix} S^{-1}(\tau).$$

The adiabatic basis is defined as $|\tilde{\rho}(\tau)\rangle\rangle = S^{-1}(\tau)|\rho(\tau)\rangle\rangle$. In this adiabatic basis, the master equation takes

$$\frac{d}{d\tau} |\tilde{\rho}(\tau)\rangle\rangle \sim \begin{pmatrix} \chi_1(\tau) & 0 & 0 & 0 \\ 0 & \chi_2(\tau) & 0 & 0 \\ 0 & 0 & \chi_3(\tau) & 0 \\ 0 & 0 & 0 & \chi_4(\tau) \end{pmatrix} |\tilde{\rho}(\tau)\rangle\rangle.$$

The approximation is referred adiabatic approximation and is effective in the region where $\kappa \gg 1$. Using the initial conditions $\rho_{11}(\tau_i) = 1$, $\rho_{12}(\tau_i) = \rho_{21}(\tau_i) = \rho_{22}(\tau_i) = 0$ and the conditions $\tau_i \rightarrow -\infty$ and $\tau_f \rightarrow \infty$, transition probability is approximated as

$$\langle \overline{P(\tau_f)} \rangle^{(ii),(iii)} \sim \frac{1}{2} (1 - \exp(-4\pi\lambda\kappa)). \quad (10)$$

This is the approximate solution when $\kappa \gg 1$.

C. Approximate solution for the transition probability

Connecting the approximation Eq. (9) derived in the regions (i) and (ii) with the approximation Eq. (10) derived in the regions (ii) and (iii), the effective transition probability in the regions (i), (ii), and (iii) is expressed as

$$\langle \overline{P(\tau_f)} \rangle^{\text{all}} \sim p^{\text{non-ad}}(\kappa) + p^{\text{ad}}(\lambda, \kappa), \quad (11)$$

$$p^{\text{non-ad}}(\kappa) = e^{-2\pi\kappa},$$

$$p^{\text{ad}}(\lambda, \kappa) = \frac{1}{2} (1 - \exp(-4\pi\lambda\kappa)).$$

This coincides with Eq. (9) to the first-order perturbation of λ . Fig. 3 displays the numerical result obtained from solving the master equation Eq. (6) and the approximation solutions Eq. (11).

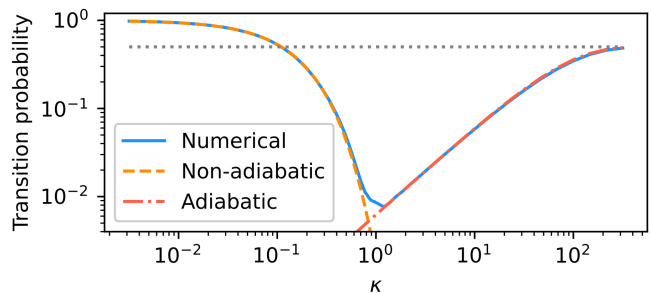


FIG. 3. Plots of the transition probabilities at τ_f against κ . The blue line (Numerical) represents the numerical simulation of Eq. (6) over the time span from $\tau_i = -200$ to $\tau_f = 200$. The yellow dashed line (Non-adiabatic) represents $p^{\text{non-ad}}$, while the red dashed line (Adiabatic) represents p^{ad} , with $\lambda = 10^{-3}$. The gray dot line represents $1/2$.

It becomes apparent that the non-adiabatic approximation solution is effective in the small κ region, while the adiabatic approximation solution is effective in the large κ region. We illustrate the comparison between the numerically derived transition probability and $p^{\text{non-ad}} + p^{\text{ad}}$ in the $\kappa \sim 1$ domain in Fig. 4.

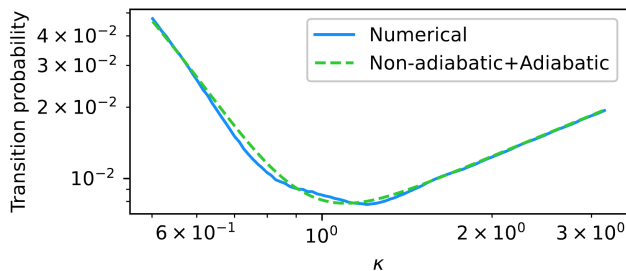


FIG. 4. Plots of the transition probabilities at τ_f against κ , focusing around $\kappa = 1$. The blue line (Numerical) represents the numerical simulation of Eq. (6) over the time interval from $\tau_i = -200$ to $\tau_f = 200$. The green dashed line (Non-adiabatic+Adiabatic) represents $p^{\text{non-ad}} + p^{\text{ad}}$, with $\lambda = 10^{-3}$.

While we have not found a precise solution near $\kappa \sim 1$, it is confirmed that Eq. (11) does not significantly deviate from the numerical results. The behavior of the transition probability in the regime where κ is sufficiently large is provided in Appendix E.

III. TRANSVERSE FIELD ISING CHAIN WITH GAUSSIAN WHITE NOISE

In Sec. II, We have considered a system involving the two-level Landau–Zener model with Gaussian white noise to analyze transition probability. In this section, we extend this theoretical framework to apply it to the transverse field Ising model following the approach [3]. The Hamiltonian is described as

$$H_{\text{IC}}(t) = -\frac{1}{2} \sum_{j=1}^N \left(\left(\frac{vt}{2} + \gamma(t) \right) \sigma_j^z + J \sigma_j^x \sigma_{j+1}^x \right). \quad (12)$$

Here, a periodic boundary condition $\sigma_{N+1}^a = \sigma_1^a$ is imposed. We consider a sufficiently large number of spins N , corresponding to a thermodynamic limit. For simplicity, we assume N is an even number. In the adiabatic regime, where κ is large, we seek the defect density and verify its scaling. Taking the initial state as the ground state of this Hamiltonian, the state evolves under this Hamiltonian H_{IC} . The initial state at initial time $\tau_i \sim -\infty$ consists of spin-down particles $|\psi(\tau_i)\rangle = |\downarrow\rangle_j^{\otimes N}$, where $\sigma_j^z |\downarrow\rangle_j = -|\downarrow\rangle_j$. The ground state at the final time $\tau_f \sim \infty$ consists of spin-up particles $|\uparrow\rangle_j^{\otimes N}$. The defect density corresponds to the density of spin-down particles at the final time. The aim is to derive analytically the defect density at the final time. Here, we introduce the spinless fermion operator \hat{c}_j and perform the Jordan-Wigner transformation as

$$\sigma_j^z = 1 - 2\hat{c}_j^\dagger \hat{c}_j, \quad \sigma_j^x = \left(\hat{c}_j^\dagger + \hat{c}_j \right) \prod_{l < j} (-\sigma_l^z).$$

The operators \hat{c}_j satisfy the anticommutation relations $\{\hat{c}_j, \hat{c}_k^\dagger\} = \delta_{jk}$ and $\{\hat{c}_j, \hat{c}_k\} = \{\hat{c}_j^\dagger, \hat{c}_k^\dagger\} = 0$. When op-

erating $\prod_{j=1}^N \sigma_j^z$ on the initial state, the eigenvalue is 1. It indicates \hat{c}_j follows the anti-periodic boundary conditions $\hat{c}_{N+1} = -\hat{c}_1$ [3]. Therefore, performing the Fourier transform of the operator \hat{c}_j , we obtain

$$\hat{c}_j = \frac{1}{\sqrt{N}} e^{-i\frac{\pi}{4}} \sum_q e^{-iqj} \hat{c}_q,$$

where $q = \pm(2n-1)\pi/N$, $n \in 1, \dots, N/2$. Using the operators \hat{c}_q , the Hamiltonian Eq. (12) can be expressed as

$$H_{\text{IC}}(t) = \sum_{q>0} (\hat{c}_q^\dagger \hat{c}_{-q}) (h_q(t) + h_{\text{noise}}(t)) \begin{pmatrix} \hat{c}_q \\ \hat{c}_{-q}^\dagger \end{pmatrix}, \quad (13)$$

where

$$h_q(t) = \left(\frac{vt}{2} + J \cos q \right) \sigma^z + J \sin q \sigma^x,$$

$$h_{\text{noise}}(t) = \gamma(t) \sigma^z.$$

We define the states as $|\uparrow\rangle_q = \hat{c}_q^\dagger \hat{c}_{-q}^\dagger |0\rangle_q$ and $|\downarrow\rangle_q = |0\rangle_q$, where $|0\rangle_q$ represents the normalized vacuum state for mode q , satisfying $\hat{c}_q |0\rangle_q = \hat{c}_{-q} |0\rangle_q = 0$. The ground state at infinite past for mode q is obtained by $|\uparrow\rangle_q^{\otimes q > 0}$ from Eq. (13). Since the Hamiltonian is separable into sums for each mode q and the total sum of q remains conserved, the density operator at any time t can be decomposed as

$$\hat{\rho}(t) = \bigotimes_{q>0} \hat{\rho}_q(t).$$

Here, $\hat{\rho}_q$ is a density operator constructed only from $|\uparrow\rangle_q$ and $|\downarrow\rangle_q$. For the initial conditions in mode q , we select the pure state of the ground state $|\uparrow\rangle_q \langle \uparrow|$. The density operator $\hat{\rho}_q(t)$ is represented in matrix form as

$$\rho_q(t) = \begin{pmatrix} \langle \uparrow | \hat{\rho}_q(t) | \uparrow \rangle_q & \langle \uparrow | \hat{\rho}_q(t) | \downarrow \rangle_q \\ \langle \downarrow | \hat{\rho}_q(t) | \uparrow \rangle_q & \langle \downarrow | \hat{\rho}_q(t) | \downarrow \rangle_q \end{pmatrix}.$$

The density matrix $\rho_q(t)$ evolves under the Hamiltonian $h_q(t) + h_{\text{noise}}(t)$. The transition probability in mode q at time t is expressed using the time evolution operator $U_q(t, t_i)$ and the noise-averaged density matrix $\overline{\rho_q(t)}$ as

$$\begin{aligned} \langle \overline{P_q(t)} \rangle &= \text{Tr} \left[\overline{\rho_q(t)} P_q \right] \\ &= \text{Tr} \left[U_q(t, t_i) \rho_q(t_i) U_q^\dagger(t, t_i) P_q \right], \end{aligned}$$

where $P_q = \text{diag}(1, 0)$, which corresponds to $|\uparrow\rangle_q \langle \uparrow|$. Similar to Sec. II, the noise-averaged density matrix $\rho_q(t)$ satisfies the master equation

$$\frac{d}{dt} \overline{\rho_q(t)} = -i \left[h_q(t), \overline{\rho_q(t)} \right] + \frac{1}{2} W^2 \left[\left[\sigma^z, \overline{\rho_q(t)} \right], \sigma^z \right].$$

The differences with Eq. (2) involve a time shift in $h_q(t)$ compared to $H_0(t)$, and the modification of the coupling term from J in $H_0(t)$ to $J \sin q$ in $h_q(t)$. Considering the initial and final times extending to the infinite past and future, the time shift in $h_q(t)$ can be neglected. The dimensionless master equation is expressed as

$$\begin{aligned} \frac{d}{d\tau} \overline{\rho_q(\tau)} &= -i \left[\tilde{h}_q(\tau), \overline{\rho_q(\tau)} \right] + \frac{\lambda}{2} \sqrt{\kappa} \left[\left[\sigma^z, \overline{\rho_q(\tau)} \right], \sigma^z \right], \\ \tilde{h}_q(\tau) &= \frac{\tau}{2} \sigma^z + \sqrt{\kappa_q} \sigma^x, \\ \kappa_q &= \kappa \sin^2 q. \end{aligned}$$

This master equation is similar to Eq. (4). The parameter κ_q satisfies the conditions $\kappa_{\frac{\pi}{2}} = \kappa$ and $\kappa_q \leq \kappa = J^2/v$. In the vicinity of $q \sim 0, \pi$, the energy gap diminishes, indicating the non-adiabatic regime. Whereas elsewhere, a significant energy gap prevails, indicating the adiabatic domain.

Subsequently, we consider the adiabatic regime. Using the transition probability of q mode, we calculate the defect density. As the state $|\uparrow\rangle_q$ denotes a two-particle state, the expected defects number is twice the transition probability. Consequently, the expected defects number at the final time τ_f can be expressed as

$$\langle \mathcal{N}(\tau_f) \rangle = 2 \sum_{q>0} \left| \langle \overline{P_q(\tau_f)} \rangle \right|^2.$$

In the thermodynamic limit, the normalized expectation value of defects can be approximated as

$$n(\tau_f) = \frac{\langle \mathcal{N}(\tau_f) \rangle}{N} \rightarrow \int_0^\pi \frac{dq}{\pi} \left| \langle \overline{P_q(\tau_f)} \rangle \right|^2, \quad (14)$$

where $\sum_{q>0} \rightarrow \int_0^\pi \frac{dq}{2\pi}$ is used. By using the result of the Landau-Zener model, we obtain the transition probability at final time $\tau_f \sim \infty$ as

$$\begin{aligned} \left| \langle \overline{P_q(\tau_f)} \rangle \right|^2 &\sim l^{\text{non-ad}}(q) + l^{\text{ad}}(q), \\ l^{\text{non-ad}}(q) &= e^{-2\pi\kappa_q}, \\ l^{\text{ad}}(q) &= \frac{1}{2} (1 - \exp(-4\pi\lambda\sqrt{\kappa}\sqrt{\kappa_q})). \end{aligned} \quad (15)$$

We present plots showing both the numerical results and the approximate solution Eq. (15) in Fig. 5. The Numerical result converges to $l^{\text{non-ad}}(q)$ when q is close to 0 or π , while it converges to $l^{\text{ad}}(q)$ elsewhere. Therefore, Eq. (15) provides an approximate solution and its integration yields an approximation of the defect.

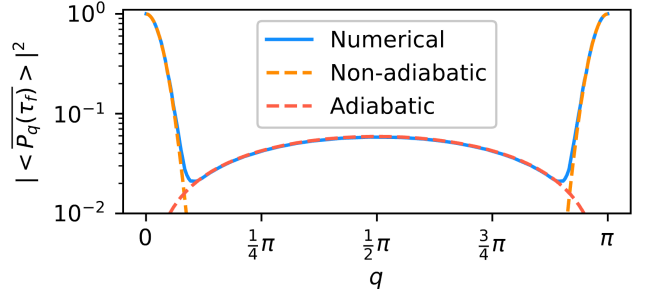


FIG. 5. Plots of the transition probability $\left| \langle \overline{P_q(\tau_f)} \rangle \right|^2$ against q . The blue line (Numerical) represents the numerical simulation of Eq. (6) over the time span from $\tau_i = -200$ to $\tau_f = 200$. The yellow dashed line (Non-adiabatic) represents $l^{\text{non-ad}}(q)$, while the red dashed line (Adiabatic) represents $l^{\text{ad}}(q)$, with $\lambda = 10^{-3}$.

Using Eq. (15), the defect density $n(\lambda, \kappa)$ can be approximated as

$$n^{\infty\text{-order}}(\lambda, \kappa) = n^{\text{KZM}}(\kappa) + n^{\text{noise}}(\lambda, \kappa),$$

$$\begin{aligned} n^{\text{KZM}}(\kappa) &= \int_0^\pi \frac{dq}{\pi} l^{\text{non-ad}}(q) = \int_0^\pi \frac{dq}{\pi} e^{-2\pi\kappa \sin^2 q} \\ &\sim 2 \int_0^\infty \frac{dq}{\pi} e^{-2\pi\kappa q^2} = \frac{1}{\pi\sqrt{2\kappa}}, \end{aligned} \quad (16)$$

$$\begin{aligned} n^{\text{noise}}(\lambda, \kappa) &= \int_0^\pi \frac{dq}{\pi} l^{\text{ad}}(q) \\ &= \int_0^\pi \frac{dq}{\pi} \left(\frac{1}{2} - \frac{1}{2} \exp(-4\pi\lambda\kappa |\sin q|) \right) \\ &= \frac{1}{2} - \frac{1}{2} I_0(4\pi\lambda\kappa) + \frac{1}{2} L_0(4\pi\lambda\kappa) \end{aligned}$$

Here, the condition $\kappa \gg 1$ is used in the calculation of Eq. (16). Consequently, the approximate solution $n^{\infty\text{-order}}$ is valid only in the regime $\kappa \gg 1$. $I_0(z)$ is the modified Bessel function of the first kind and $L_0(z)$ is the modified Struve function [47]. $n^{\text{KZM}}(\kappa)$ represents the defect density in the absence of noise and corresponds with the result from the QKZM. n^{noise} denotes the contribution due to the influence of Gaussian white noise. $n^{\infty\text{-order}}$ includes contributions up to infinite order with respect to λ . By using the asymptotic conditions of $I_0(z)$ and $L_0(z)$, $n^{\infty\text{-order}} \rightarrow 1/2$ can be verified when $\lambda\kappa \rightarrow \infty$. This implies that the system asymptotically approaches the infinite-temperature state as the noise becomes large. In contrast, when $\lambda\kappa \ll 1$, using the properties $I_0(z) = 1 + \frac{z^2}{4} + \mathcal{O}(z^4)$ and $L_0(z) = \frac{2z}{\pi} + \mathcal{O}(z^3)$, we can further refine the expression

$$n^{\infty\text{-order}}(\lambda, \kappa) \sim \frac{1}{\pi\sqrt{2\kappa}} + 4\lambda\kappa =: n^{\text{1st}}(\lambda, \kappa). \quad (17)$$

The second term in n^{1st} is proportional to $W^2 \propto \lambda$, which is expected from computational researches [12, 13].

Eq. (17) demonstrates the successful reproduction of the anti-KZM scaling. In the absence of Gaussian white noise, a larger κ , i.e., a smaller v , leads to a smaller defect density as expected by QKZM. However, when Gaussian white noise is induced, the defect density increases in the region where κ is large. The second term diverges as $\kappa \rightarrow \infty$, which is due to neglecting higher-order contributions of $\lambda\kappa$. Incorporating these higher-order λ contributions improves the accuracy of the approximation. The approximate solution including contributions up to the second order with respect to λ is given by

$$\begin{aligned} n^{\infty\text{-order}}(\lambda, \kappa) &\sim \frac{1}{\pi\sqrt{2\kappa}} + 4\lambda\kappa - 2\pi^2\lambda^2\kappa^2 \\ &=: n^{2\text{nd}}(\lambda, \kappa). \end{aligned} \quad (18)$$

The results of the defect density n obtained numerically, along with $n^{\infty\text{-order}}$, $n^{1\text{st}}$, and $n^{2\text{nd}}$ are compared in Fig. 6. The spin number N is chosen to be a large, specifically $N = 100$. λ is smaller in the upper figure.

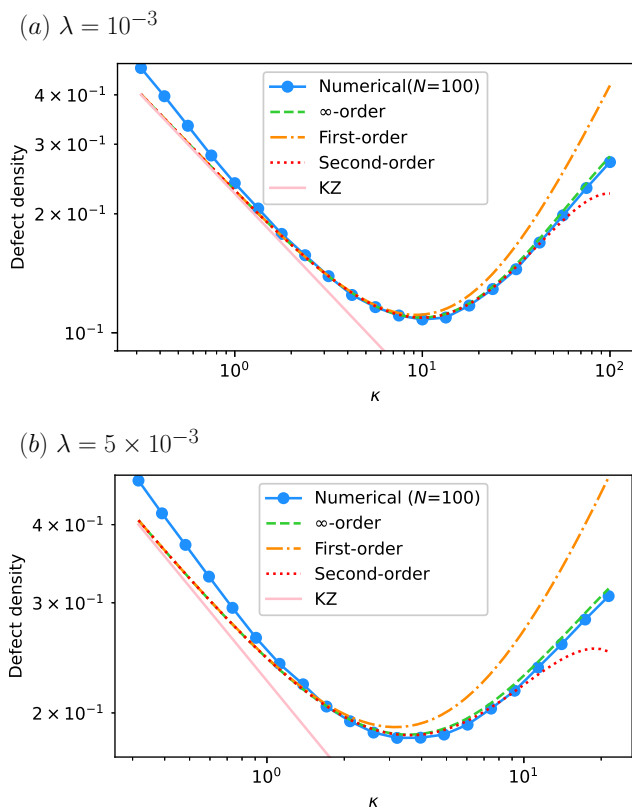


FIG. 6. Plots of the defect density against κ . The upper (a) corresponds to $\lambda = 10^{-3}$, while the lower (b) corresponds to $\lambda = 5 \times 10^{-3}$. The blue solid lines (Numerical) represent the numerical simulation of Eq. (6) over the time span $\tau_i = -200$ to $\tau_f = 200$, plotting the discrete sum in Eq. (14) with $N = 100$. The green dashed lines (∞ -order) represent $n^{\infty\text{-order}}$, the yellow dashed lines (First-order) represent $n^{1\text{st}}$, and the red dot lines (Second-order) represent $n^{2\text{nd}}$. The pink solid lines (KZ) represent n^{KZM} .

It has been verified that $n^{\infty\text{-order}}$ closely matches the defect density n in the region where κ is large, which is adiabatic region. In the region where κ is small, the approximation used to perform the integration for deriving n^{KZM} becomes less effective, and $n^{\infty\text{-order}}$ is not a suitable approximation. Both $n^{1\text{st}}$ and $n^{2\text{nd}}$ serve as approximate solutions to $n^{\infty\text{-order}}$ when κ is small. It is observed that the region where the approximation is effective for $n^{2\text{nd}}$ is larger than that for $n^{1\text{st}}$. Hence, we have successfully obtained a new scaling $n^{2\text{nd}}$. As λ increases, the κ which represents the location of the minimum becomes smaller and the validity of $n^{1\text{st}}$ in its neighborhood becomes worse. The behavior of the defect density in the regime where κ is sufficiently large is provided in Appendix E.

IV. THE DERIVATION OF THE OPTIMIZATION PARAMETER

Let v_{opt} denote the value at which the defect density n attains its minimum. The previous studies [12, 13] numerically seek the minimum of the defect density n and obtain the scaling of v_{opt} with respect to $W^2 \propto \lambda$. We seek the approximation of v_{opt} through the critical point. As defined by $\kappa_{\text{min}}^{1\text{st}} = (2^7\pi^2\lambda^2)^{-\frac{1}{3}}$, the derivative is obtained by

$$\left. \frac{d}{d\kappa} n^{1\text{st}} \right|_{\kappa=\kappa_{\text{min}}^{1\text{st}}} = -\frac{1}{\pi(2\kappa_{\text{min}}^{1\text{st}})^{\frac{3}{2}}} + 4\lambda = 0. \quad (19)$$

The critical point of $n^{1\text{st}}$ is $\kappa = \kappa_{\text{min}}^{1\text{st}}$, where $n^{1\text{st}}$ attains its minimum value. Since $\kappa = J^2/v$, v_{opt} for $n^{1\text{st}}$ is given by

$$v_{\text{opt}}^{1\text{st}}/J^2 = (2^7\pi^2\lambda^2)^{\frac{1}{3}}.$$

Therefore, similar to the previous study [13], we have demonstrated $v_{\text{opt}}^{1\text{st}} \propto \lambda^{\frac{2}{3}} \propto W^{\frac{4}{3}}$. Next, we choose $n^{2\text{nd}}$ as an approximate solution for the defect density n . The critical point $\kappa^{2\text{nd}}$ cannot be determined analytically. We make an assumption that $\kappa^{2\text{nd}}$ is close to $\kappa_{\text{min}}^{1\text{st}}$. We determine $\kappa^{2\text{nd}}$ as the perturbation from $\kappa_{\text{min}}^{1\text{st}}$. Setting $\kappa_{\text{min}}^{2\text{nd}} = \kappa_{\text{min}}^{1\text{st}}(1 + \varepsilon)$, the derivative is expressed as

$$\begin{aligned} &\left. \frac{d}{d\kappa} n^{2\text{nd}} \right|_{\kappa=\kappa_{\text{min}}^{2\text{nd}}} \\ &= -\frac{1}{\pi(2\kappa_{\text{min}}^{2\text{nd}})^{\frac{3}{2}}} + 4\lambda - 4\pi^2\lambda^2\kappa_{\text{min}}^{2\text{nd}} \\ &= -\frac{1}{\pi(2\kappa_{\text{min}}^{1\text{st}})^{\frac{3}{2}}}(1 + \varepsilon)^{-\frac{3}{2}} + 4\lambda - 4\pi^2\lambda^2\kappa_{\text{min}}^{1\text{st}}(1 + \varepsilon). \end{aligned}$$

Assuming ε to be sufficiently small, incorporating perturbations up to the first order in ε yields

$$\left. \frac{d}{d\kappa} n^{2\text{nd}} \right|_{\kappa=\kappa_{\text{min}}^{2\text{nd}}} \sim \frac{3\varepsilon}{2\pi(2\kappa_{\text{min}}^{1\text{st}})^{\frac{3}{2}}} - 4\pi^2\lambda^2\kappa_{\text{min}}^{1\text{st}}(1 + \varepsilon).$$

Here, Eq. (19) is utilized. For the right-hand side to be zero, ε is represented as

$$\varepsilon = \frac{1}{3} \left(\frac{\pi^4 \lambda}{2^4} \right)^{\frac{1}{3}} + \mathcal{O} \left(\lambda^{\frac{2}{3}} \right).$$

Thus, ignoring $\mathcal{O} \left(\lambda^{\frac{2}{3}} \right)$, v_{opt} for n^{2nd} is expressed as

$$v_{\text{opt}}^{\text{2nd}} / J^2 = (2^7 \pi^2 \lambda^2)^{\frac{1}{3}} - \frac{2}{3} \pi^2 \lambda.$$

If selected $n^{\infty\text{-order}}$ as an approximate solution for the defect density, v_{opt} is obtained by finding numerically the minimum value as v varies. This is denoted as $v_{\text{opt}}^{\infty\text{-order}}$. By solving Eq. (6) and calculating the discrete sum in Eq. (14), the minimum values are obtained numerically for v_{opt} , $v_{\text{opt}}^{\infty\text{-order}}$, $v_{\text{opt}}^{\text{1st}}$, and $v_{\text{opt}}^{\text{2nd}}$ against λ are plotted respectively in Fig. 7.

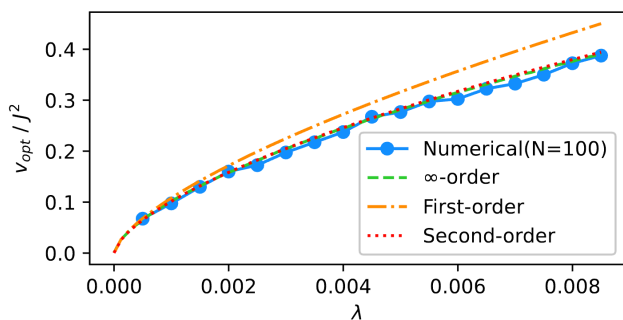


FIG. 7. Plots of v_{opt} against λ . The blue line (Numerical) represents the numerical simulation of Eq. (6) over the time span $\tau_i = -200$ to $\tau_f = 200$, plotting the discrete sum in Eq. (14), with $N = 100$. The green dashed line (∞ -order) represents $v_{\text{opt}}^{\infty\text{-order}}$, the yellow dashed line (First-order) represents $v_{\text{opt}}^{\text{1st}}$, and the red dot line (Second-order) represents $v_{\text{opt}}^{\text{2nd}}$.

It can be confirmed that $v_{\text{opt}}^{\infty\text{-order}}$ serves as an approximation of v_{opt} . Since $v_{\text{opt}}^{\text{2nd}}$ approaches the numerical results more closely than $v_{\text{opt}}^{\text{1st}}$, we suggest that $v_{\text{opt}}^{\text{2nd}}$ is more effective. The relative deviation of $v_{\text{opt}}^{\text{2nd}}$ over $v_{\text{opt}}^{\text{1st}}$ is expressed as

$$\frac{v_{\text{opt}}^{\text{2nd}}}{v_{\text{opt}}^{\text{1st}}} \sim 1 - \left(\frac{\pi^4 \lambda}{2^4 \times 3^3} \right)^{\frac{1}{3}} =: 1 - \zeta(\lambda).$$

Let the defect density in each optimized v be n_{opt} , which corresponds to the minimum value of n . The relative deviation is expressed as

$$\frac{n_{\text{opt}}^{\text{2nd}}}{n_{\text{opt}}^{\text{1st}}} \sim 1 - \left(\frac{\pi^4 \lambda}{2^{10} \times 3^3} \right)^{\frac{1}{3}} =: 1 - \xi(\lambda).$$

The magnitude of ζ and ξ indicates the effectiveness of the approximation of $v_{\text{opt}}^{\text{1st}}$ and $n_{\text{opt}}^{\text{1st}}$ respectively. If both

parameters are sufficiently small compared to 1, $v_{\text{opt}}^{\text{1st}}$ and $n_{\text{opt}}^{\text{1st}}$ can be considered effective. For example, when $\lambda = 10^{-3}$, $\zeta \approx 0.061$ and $\xi \approx 0.015$. When $\lambda = 5 \times 10^{-3}$, $\zeta \approx 0.10$ and $\xi \approx 0.026$. We see that as λ increases, ζ and ξ increase. This leads to a loss of validity of the first-order approximation in the regime of large λ . However, if $\lambda \gtrsim 0.01$, approximation formulas break down. This is because, as λ increases, the critical point of κ decreases and the approximation utilized to perform the integration in Eq. (16) becomes less effective near the critical point.

V. CONCLUSION

Under the approximation of a small noise, $\lambda \ll 1$, we analytically derived the transition probability of the Landau–Zener model with Gaussian white noise. We considered three κ regions: (i) small, (ii) medium, and (iii) large. For the regions (i) and (ii), we solved a master equation under a first-order approximation for λ . This involved performing integrals of products of special functions, and the feasibility of these integrals depends strongly on the system. Hence, it is anticipated that this method may not be applied to other systems. However, by selecting parameters that asymptotically approach those of the system we addressed, we suggested that other systems may converge to the solutions obtained in this research. For the regions (ii) and (iii), we employed an adiabatic approximation method, which is considered to be useful in various other systems.

Applying the analysis of the Landau–Zener model, we analytically derived the defect density in the transverse field Ising model with Gaussian white noise. The results reveal that in the regime where $\kappa \ll 1/\lambda$, the anti-KZM scaling previously known through numerical computations [12, 13] is effective. Furthermore, the optimal parameter v_{opt} follows the same scaling as the anti-KZM previously known. On the other hand, in the region where $1/\lambda \ll \kappa$, a new scaling was found. It can be argued that to minimize the defect density, it is desirable to choose v_{opt} smaller than the value obtained from anti-KZM previously known in the noisy region. Furthermore, we have achieved the capability to discuss the efficacy of first-order perturbation.

While the effectiveness of the approximate solutions for $\kappa \sim 1$ has not been formally proven, they are promising approximations by compared to numerical results. Therefore, further investigation is necessary to confirm the reason. Additionally, we aim at extending the methodology employed in this study to other systems such as XY chain models.

As an application to another system, we consider the Schwinger mechanism [48–50], where electron-positron pairs are expected to be generated when an electric field is applied to a vacuum. Since the time evolution of this system is related to the Landau–Zener system, we propose applying the methods of this research to derive the number density of electron-positron pairs generated by

an electric field, accounting for the influence of noise. It is anticipated that, due to the induced noise, the number of generated electrons significantly increases as the dynamically assisted Schwinger mechanism [51].

ACKNOWLEDGEMENT

We thank H. Nakazato for helpful discussions. T.S. was supported by Japan's MEXT Quantum Leap Flagship Program Grant No. JPMXS0120319794.

Appendix A: The derivation of the transition probability with perturbation

We derive the first-order approximation solution Eq. (7) for the perturbation. $f(\tau_f, \tau_i)$ and $g(\tau_f, \tau_i)$ are components of the time evolution operator $U_0(\tau, \tau_i)$. These are obtained analytically and are expressed as linear combinations of parabolic cylinder functions [47] as Eq. (5). The transition probability is expressed up to first order in λ as

$$\begin{aligned} \langle \overline{P(\tau_f)} \rangle &= |f(\tau_f, \tau_i)|^2 - 4\lambda\sqrt{\kappa}(|f(\tau_f, \tau_i)|^2 - |g(\tau_f, \tau_i)|^2) \int_{\tau_i}^{\tau_f} d\tau |f(\tau, \tau_i)|^2 |g(\tau, \tau_i)|^2 \\ &\quad + 4\lambda\sqrt{\kappa} \operatorname{Re} \left(f(\tau_f, \tau_i) g(\tau_f, \tau_i) \int_{-\infty}^{\infty} d\tau f^*(\tau, \tau_i) g^*(\tau, \tau_i) (|f(\tau, \tau_i)|^2 - |g(\tau, \tau_i)|^2) \right). \end{aligned}$$

Using the equations for a positive value of τ

$$D_{i\kappa} \left(e^{\frac{3\pi}{4}i\tau} \right) \sim e^{\frac{i}{4}\tau^2} e^{-\frac{3\pi}{4}\kappa} \tau^{i\kappa} + \mathcal{O}(\tau^{-1}),$$

$$D_{-i\kappa} \left(e^{\frac{\pi}{4}i\tau} \right) \sim e^{-\frac{i}{4}\tau^2} e^{\frac{\pi}{4}\kappa} \tau^{-i\kappa} + \mathcal{O}(\tau^{-1}),$$

$$D_{-i\kappa-1} \left(e^{\frac{5\pi}{4}i\tau} \right) \sim \frac{\sqrt{2\pi}}{\Gamma(i\kappa+1)} e^{\frac{i}{4}\tau^2} e^{-\frac{\pi}{4}\kappa} \tau^{i\kappa} + \mathcal{O}(\tau^{-1}),$$

$$D_{i\kappa-1} \left(e^{-\frac{\pi}{4}i\tau} \right) \sim \mathcal{O}(\tau^{-1}),$$

$|\Gamma(1-ix)|^2 = \frac{\pi x}{\sinh(\pi x)}$ and limiting $\tau_i \rightarrow -\infty$, $\tau_f \rightarrow \infty$, the transition probability is obtained as

$$\tilde{X}(\tau) = \frac{\sqrt{2\pi\kappa}}{\Gamma(1+i\kappa)} e^{-2\pi\kappa} D_{i\kappa}(e^{-\frac{i\pi}{4}\tau}) \sqrt{\kappa} D_{i\kappa-1}(e^{-\frac{i\pi}{4}\tau}), \quad \tilde{Y}(\tau) = e^{-\frac{\pi\kappa}{2}} (|D_{i\kappa}(e^{-\frac{i\pi}{4}\tau})|^2 - |\sqrt{\kappa} D_{i\kappa-1}(e^{-\frac{i\pi}{4}\tau})|^2),$$

$$\langle \overline{P(\tau_f)} \rangle = e^{-2\pi\kappa} + 4\lambda\sqrt{\kappa} \int_{-\infty}^{\infty} d\tau \left(\frac{1-2e^{-2\pi\kappa}}{1-e^{-2\pi\kappa}} e^{2\pi\kappa} |\tilde{X}(\tau)|^2 + \operatorname{Re}(\tilde{X}(\tau)) \tilde{Y}(\tau) \right).$$

Using the formula $\frac{\sqrt{2\pi}}{\Gamma(\nu+1)} D_\nu(z) = e^{-\frac{i\pi\nu}{2}} D_{-\nu-1}(-iz) + e^{\frac{i\pi\nu}{2}} D_{-\nu-1}(iz)$, we obtain Eq. (7).

is approximated as

Appendix B: The derivation of approximation with perturbation

We demonstrate Eq. (8) in the region (ii) ($1 \ll \kappa \ll \frac{1}{\lambda}$). The approximate solution for the transition probability

$$\begin{aligned} \langle \overline{P(\tau_f)} \rangle &\sim 4\lambda\sqrt{\kappa} e^{-\pi\kappa} \kappa^2 \\ &\quad \times \int_{-\infty}^{\infty} d\tau \left| D_{-i\kappa-1}(e^{\frac{i\pi}{4}\tau}) D_{-i\kappa-1}(-e^{\frac{i\pi}{4}\tau}) \right|^2. \end{aligned}$$

To perform this calculation, we utilize the following formula [52]

$$D_{-\nu}(z)D_{-\nu}(-z) = \frac{2e^{\frac{\kappa^2}{2}}}{\Gamma(\nu + \frac{1}{2})} \int_0^\infty dy \cos(2zy)e^{-2y^2} {}_1F_1\left(\frac{1}{2}, \nu + \frac{1}{2}, y^2\right).$$

Here ${}_1F_1$ denotes the confluent hypergeometric function. By substituting $z = e^{i\frac{\pi}{4}}\tau$ and $\nu = i\kappa + 1$, and changing

the integration path to $t = e^{i\frac{\pi}{4}}y$, we get

$$D_{-i\kappa-1}(e^{i\frac{\pi}{4}}\tau)D_{-i\kappa-1}(-e^{i\frac{\pi}{4}}\tau) = \frac{2e^{-i\frac{\pi}{4}}e^{i\frac{\kappa^2}{2}}}{\Gamma(i\kappa + \frac{3}{2})} \int_0^\infty dt \cos(2\tau t)e^{2it^2} {}_1F_1\left(\frac{1}{2}, i\kappa + \frac{3}{2}, -it^2\right).$$

Therefore, $\langle \overline{P(\tau_f)} \rangle$ is approximated as

$$\begin{aligned} \langle \overline{P(\tau_f)} \rangle &\sim 4\lambda\sqrt{\kappa}e^{-\pi\kappa}\kappa^2 \int_{-\infty}^\infty d\tau \left| D_{-i\kappa-1}(e^{i\frac{\pi}{4}}\tau)D_{-i\kappa-1}(-e^{i\frac{\pi}{4}}\tau) \right|^2 \\ &= 4\lambda\sqrt{\kappa}e^{-\pi\kappa}\kappa^2 \int_{-\infty}^\infty d\tau \frac{1}{|\Gamma(i\kappa + \frac{3}{2})|^2} \int_0^\infty dr (e^{2i\tau r} + e^{-2i\tau r})e^{2ir^2} {}_1F_1\left(\frac{1}{2}, i\kappa + \frac{3}{2}, -ir^2\right) \\ &\quad \times \int_0^\infty ds (e^{2i\tau s} + e^{-2i\tau s})e^{-2is^2} {}_1F_1\left(\frac{1}{2}, -i\kappa + \frac{3}{2}, is^2\right). \end{aligned}$$

We change the order of integration, performing the integration over τ first. Utilizing the conditions that r and s are positive, we employ the formulas $\int_{-\infty}^\infty d\tau e^{2i\tau(r-s)} = \pi\delta(r-s)$ and $\int_{-\infty}^\infty d\tau e^{2i\tau(r+s)} = 0$. Consequently, we get

$$\begin{aligned} \langle \overline{P(\tau_f)} \rangle &\sim 4\lambda\sqrt{\kappa} \frac{2\pi}{|\Gamma(i\kappa + \frac{3}{2})|^2} e^{-\pi\kappa}\kappa^2 \\ &\quad \times \int_0^\infty dr \left| {}_1F_1\left(\frac{1}{2}, i\kappa + \frac{3}{2}, -ir^2\right) \right|^2. \end{aligned}$$

Note that this derivation is based on the assumption of infinite time integration. Therefore, this relationship cannot be applied in systems where the time span is finite. Furthermore, using the following formula

$$\frac{2\pi}{|\Gamma(i\kappa + \frac{3}{2})|^2} e^{-\pi\kappa}\kappa^2 = \frac{\kappa^2}{\kappa^2 + \frac{1}{4}} (1 + e^{-2\pi\kappa})$$

and the approximations $e^{-2\pi\kappa} \ll 1$ and $\kappa^2 \gg \frac{1}{4}$, the transition probability is expressed as

$$\langle \overline{P(\tau_f)} \rangle \sim 4\lambda\sqrt{\kappa} \int_0^\infty dr \left| {}_1F_1\left(\frac{1}{2}, i\kappa + \frac{3}{2}, -ir^2\right) \right|^2.$$

By employing the variable transformation $r = \sqrt{\kappa}x$, the expression can be rewritten as

$$\langle \overline{P(\tau_f)} \rangle \sim 4\lambda\kappa \int_0^\infty dx \left| {}_1F_1\left(\frac{1}{2}, i\kappa + \frac{3}{2}, -i\kappa x^2\right) \right|^2.$$

Furthermore, when κ is large,

$${}_1F_1\left(\frac{1}{2}, i\kappa + \frac{3}{2}, -i\kappa x^2\right) \sim \frac{1}{\sqrt{1+x^2}}. \quad (\text{B1})$$

We confirm in Appendix C that the approximate formula Eq. (B1) is effective when κ is large. Consequently, by utilizing

$$\int_0^\infty dt \frac{1}{1+x^2} = \frac{\pi}{2},$$

we can demonstrate the validity of Eq. (8).

Appendix C: The approximation of the special function

As stated in Appendix B, the approximation formula Eq. (B1) is shown to be effective when κ is large. By the properties of a confluent hypergeometric function [47]

$$\frac{d}{dz} {}_1F_1(a, b, z) = \frac{a}{b} {}_1F_1(a+1, b+1, z)$$

and

$$\begin{aligned} {}_1F_1(a, b, z) &= \frac{b-a-z-1}{b} {}_1F_1(a+1, b+1, z) \\ &\quad + \frac{a+1}{b} {}_1F_1(a+2, b+1, z), \end{aligned}$$

we get

$$\begin{aligned} \frac{d}{dx} \left(\sqrt{1+x} {}_1F_1\left(\frac{1}{2}, i\kappa + \frac{3}{2}, -i\kappa x\right) \right) \\ = \frac{3}{4\sqrt{1+x}(i\kappa + \frac{3}{2})} {}_1F_1\left(\frac{5}{2}, i\kappa + \frac{5}{2}, -i\kappa x\right). \end{aligned}$$

Integrating both sides with respect to x from 0 and using ${}_1F_1(a, b, 0) = 1$ yield

$${}_1F_1\left(\frac{1}{2}, i\kappa + \frac{3}{2}, -i\kappa x\right) = \frac{1}{\sqrt{1+x}}(1 + E_\kappa(x)),$$

$$E_\kappa(x) = \frac{3}{4(i\kappa + \frac{3}{2})} \int_0^x \frac{dy}{\sqrt{1+y}} {}_1F_1\left(\frac{5}{2}, i\kappa + \frac{5}{2}, -i\kappa y\right).$$

Therefore, the approximation Eq. (B1) is valid in the regime $E(x) \ll 1$. Fig. 8 plots the x -dependence of $|E_\kappa(x)|$. It can be observed $|E_\kappa(x)| \ll 1$ for large κ , confirming the validity of the approximation Eq. (B1).

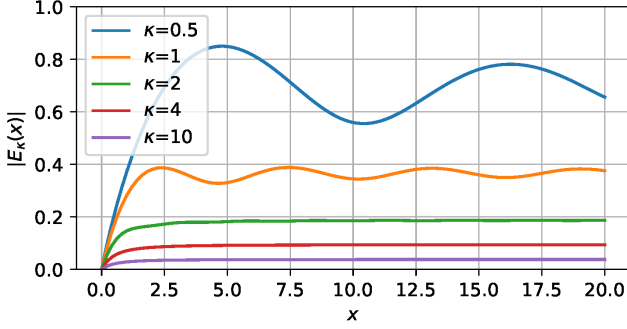


FIG. 8. Plots of $|E_\kappa(x)|$ against x . As κ increases, it is observed that this value becomes significantly smaller than 1 for any x .

Appendix D: Adiabatic approximation

In the regions (ii) and (iii) ($1 \ll \kappa$), the effectiveness of the adiabatic approximation is demonstrated. Let $|\rho(\tau)\rangle = (\rho_{11}(\tau) \ \rho_{12}(\tau) \ \rho_{21}(\tau) \ \rho_{22}(\tau))^T$. The master equation Eq. (4), is expressed as

$$|\dot{\rho}(\tau)\rangle = \mathcal{L}(\tau)|\rho\rangle. \quad (\text{D1})$$

Here, $\mathcal{L}(\tau)$ denotes the Liouvillian at time τ , which is non-Hermitian. Diagonalizing \mathcal{L} yields

$$\tilde{\mathcal{L}}(\tau) = S^{-1}(\tau)\mathcal{L}(\tau)S(\tau)$$

Here, $\tilde{\mathcal{L}}(\tau) = \text{diag}(\chi_1(\tau), \chi_2(\tau), \chi_3(\tau), \chi_4(\tau))$. $|\chi_\alpha(\tau)\rangle\rangle$ and $\langle\langle \hat{\chi}_\alpha(\tau) |$ are the normalized right eigenvectors and the normalized left eigenvectors of $\mathcal{L}(\tau)$, satisfying

$$\begin{aligned} \mathcal{L}(\tau)|\chi_\alpha(\tau)\rangle\rangle &= \chi_\alpha(\tau)|\chi_\alpha(\tau)\rangle\rangle, \\ \langle\langle \hat{\chi}_\alpha(\tau) | \mathcal{L}(\tau) &= \langle\langle \hat{\chi}_\alpha(\tau) | \chi_\alpha(\tau), \end{aligned}$$

with $\alpha = 1, 2, 3, 4$. When there is no degeneracy in the eigenvalues of the Liouvillian, meaning $\chi_\alpha \neq \chi_\beta$, the condition $\langle\langle \hat{\chi}_\alpha(\tau) | \chi_\beta(\tau)\rangle\rangle = 0$ is satisfied. Normalization is performed such that $\langle\langle \hat{\chi}_\alpha(\tau) | \chi_\beta(\tau)\rangle\rangle = \delta_{\alpha\beta}$. Expanding the state in terms of the right eigenvectors as

$$|\rho(\tau)\rangle\rangle = \sum_{\beta=1}^4 c_\beta(\tau)|\chi_\beta(\tau)\rangle\rangle, \quad (\text{D2})$$

the master equation Eq. (D1) takes

$$\begin{aligned} & \sum_{\beta=1}^4 (\dot{c}_\beta(\tau)|\chi_\beta(\tau)\rangle\rangle + c_\beta(\tau)|\dot{\chi}_\beta(\tau)\rangle\rangle) \\ &= \sum_{\beta=1}^4 c_\beta(\tau)\chi_\beta(\tau)|\chi_\beta(\tau)\rangle\rangle. \end{aligned}$$

Applying the left eigenvector $\langle\langle \hat{\chi}_\alpha(\tau) |$ yields

$$\dot{c}_\alpha(\tau) = \chi_\alpha(\tau)c_\alpha(\tau) - \sum_{\beta=1}^4 c_\beta(\tau)\langle\langle \chi_\alpha(\tau) | \dot{\chi}_\beta(\tau)\rangle\rangle.$$

Therefore, if $\langle\langle \hat{\chi}_\alpha(\tau) | \dot{\chi}_\beta(\tau)\rangle\rangle$ is sufficiently small, the equation becomes closed for α , resulting in adiabatic time evolution. $\langle\langle \chi_\alpha(\tau) | \dot{\chi}_\beta(\tau)\rangle\rangle$ has the dimension of frequency. The relevant physical frequency scale is given by the energy gap $\omega_{\alpha\beta}(\tau) = \chi_\alpha(\tau) - \chi_\beta(\tau)$. Therefore, the adiabatic condition is given by [46]

$$l_{\alpha\beta} \ll r_{\alpha\beta}, \quad (\text{D3})$$

$$l_{\alpha\beta} = \max_{\tau} |\langle\langle \hat{\chi}_\alpha(\tau) | \dot{\chi}_\beta(\tau)\rangle\rangle|, \quad r_{\alpha\beta} = \min_{\tau} |\omega_{\alpha\beta}(\tau)|.$$

Here, $r_{\alpha\beta} = r_{\beta\alpha}$. The Liouvillian under consideration is given as

$$\mathcal{L}(\tau) = \begin{pmatrix} 0 & i\sqrt{\kappa} & -i\sqrt{\kappa} & 0 \\ i\sqrt{\kappa} & -i\frac{\tau}{2} - \lambda\sqrt{\kappa} & 0 & -i\sqrt{\kappa} \\ -i\sqrt{\kappa} & 0 & i\frac{\tau}{2} - \lambda\sqrt{\kappa} & i\sqrt{\kappa} \\ 0 & -i\sqrt{\kappa} & i\sqrt{\kappa} & 0 \end{pmatrix}.$$

We calculate the eigenvalues and eigenvectors up to the first order of perturbation with respect to λ . Let $z(\tau) = \frac{\tau}{4\sqrt{\kappa}}$. The term $\mathcal{O}(\lambda^2)$ is neglected in the following analysis in this subsection. The eigenvalues and right eigenvectors of the Liouvillian are

$$\begin{aligned} \chi_1 &= 0, \\ \chi_2 &= -\frac{\lambda}{z^2+1}\sqrt{\kappa}, \\ \chi_3 &= -\frac{2z^2+1}{2z^2+2}\lambda\sqrt{\kappa} - 2i\sqrt{z^2+1}\sqrt{\kappa}, \\ \chi_4 &= -\frac{2z^2+1}{2z^2+2}\lambda\sqrt{\kappa} + 2i\sqrt{z^2+1}\sqrt{\kappa}, \end{aligned}$$

$$|\chi_1(\tau)\rangle\rangle = \begin{pmatrix} \frac{1}{\sqrt{2}} \\ 0 \\ 0 \\ \frac{1}{\sqrt{2}} \end{pmatrix},$$

$$|\chi_2(\tau)\rangle\rangle = \begin{pmatrix} \frac{z}{\sqrt{2(z^2+1)}} \\ \frac{1}{\sqrt{2(z^2+1)}} + i\lambda \frac{z\sqrt{z^2+1}}{2\sqrt{2}(z^2+1)^2} \\ \frac{1}{\sqrt{2(z^2+1)}} - i\lambda \frac{z\sqrt{z^2+1}}{2\sqrt{2}(z^2+1)^2} \\ -\frac{z}{\sqrt{2(z^2+1)}} \end{pmatrix},$$

$$|\chi_3(\tau)\rangle\rangle = \begin{pmatrix} \frac{1}{2\sqrt{z^2+1}} + i\lambda \frac{4z^2+1}{16(z^2+1)^2} \\ -\frac{1}{2} \left(1 + \frac{z}{\sqrt{z^2+1}}\right) + i\lambda \frac{3z+\sqrt{z^2+1}}{16(z^2+1)^2} \\ \frac{1}{2} \left(1 - \frac{z}{\sqrt{z^2+1}}\right) + i\lambda \frac{3z-\sqrt{z^2+1}}{16(z^2+1)^2} \\ -\frac{1}{2\sqrt{z^2+1}} - i\lambda \frac{4z^2+1}{16(z^2+1)^2} \end{pmatrix},$$

$$|\chi_4(\tau)\rangle\rangle = \begin{pmatrix} \frac{1}{2\sqrt{z^2+1}} - i\lambda \frac{4z^2+1}{16(z^2+1)^2} \\ \frac{1}{2} \left(1 - \frac{z}{\sqrt{z^2+1}}\right) - i\lambda \frac{3z-\sqrt{z^2+1}}{16(z^2+1)^2} \\ -\frac{1}{2} \left(1 + \frac{z}{\sqrt{z^2+1}}\right) - i\lambda \frac{3z+\sqrt{z^2+1}}{16(z^2+1)^2} \\ -\frac{1}{2\sqrt{z^2+1}} + i\lambda \frac{4z^2+1}{16(z^2+1)^2} \end{pmatrix}.$$

Here, the tight eigenvectors are chosen such that they satisfy $l_{\alpha\beta} = l_{\beta\alpha}$ up to the first order of λ . The eigenvector corresponding to the eigenvalue $\chi_1 = 0$ is independent of the time τ and is considered to be the infinite-temperature state. This state implies that both the probability of transitioning and the probability of not transitioning are 1/2. The 4×4 matrix $S(\tau)$ is defined as

$$S(\tau) = (|\chi_1(\tau)\rangle\rangle \quad |\chi_2(\tau)\rangle\rangle \quad |\chi_3(\tau)\rangle\rangle \quad |\chi_4(\tau)\rangle\rangle).$$

Based on this, the inverse matrix $S^{-1}(\tau)$ can also be obtained as

$$S^{-1}(\tau) = \begin{pmatrix} \langle\langle\chi_1(\tau)| \\ \langle\langle\chi_2(\tau)| \\ \langle\langle\chi_3(\tau)| \\ \langle\langle\chi_4(\tau)| \end{pmatrix}.$$

First, We verify the adiabatic condition Eq. (D3). From $l_{12}(\tau) = l_{13}(\tau) = l_{14}(\tau) = 0$, the state $|\chi_1(\tau)\rangle\rangle$ is adiabatic. By calculating other states, the following results are obtained. Up to the first order of λ , $l_{23}(\tau) = l_{24}(\tau) = \frac{1}{4\sqrt{2}\kappa}$ and $r_{23}(\tau) = r_{24}(\tau) = 2\sqrt{\kappa}$, as well as $l_{34}(\tau) = \frac{\lambda}{50\sqrt{5}\kappa}$ and $r_{34}(\tau) = 4\sqrt{\kappa}$. Therefore, the adiabatic condition is $\kappa \gg 1$.

Second, we calculate the transition probability $\tilde{\rho}(\tau_f)_{11}$ under the adiabatic approximation condition. From Eq. (D2), the adiabatic basis is defined as

$$|\tilde{\rho}(\tau)\rangle\rangle = S^{-1}(\tau)|\rho(\tau)\rangle\rangle = (c_1(\tau) \quad c_2(\tau) \quad c_3(\tau) \quad c_4(\tau))^T,$$

Under the adiabatic approximation, the differential equation is expressed as

$$\dot{c}_\alpha(\tau) \sim \chi_\alpha(\tau)c_\alpha(\tau).$$

Therefore, $c_\alpha(\tau)$ is given by

$$c_\alpha(\tau) = c_\alpha(\tau_i) \exp\left(\int_{\tau_i}^{\tau} d\tau' \chi_\alpha(\tau')\right),$$

The initial condition is $|\rho(\tau_i)\rangle\rangle = (1 \ 0 \ 0 \ 0)^T$. In the limit $\tau_i \rightarrow -\infty$, the initial conditions in the adiabatic basis are given by $c_1(\tau_i) = \frac{1}{\sqrt{2}}$, $c_2(\tau_i) = -\frac{1}{\sqrt{2}}$, $c_3(\tau_i) = c_4(\tau_i) = 0$. When evolved up to time τ , the state can be approximated in the original basis as

$$\begin{aligned} |\rho(\tau)\rangle\rangle &\sim S(\tau) \begin{pmatrix} \frac{1}{\sqrt{2}} \\ -\frac{1}{\sqrt{2}} \exp\left(-\int_{\tau_i}^{\tau} d\tau' \frac{\lambda\sqrt{\kappa}}{z^2(\tau')+1}\right) \\ 0 \\ 0 \end{pmatrix} \\ &= \frac{1}{2} \begin{pmatrix} 1 - \frac{z(\tau)}{\sqrt{z^2(\tau)+1}} \exp\left(-\int_{\tau_i}^{\tau} d\tau' \frac{\lambda\sqrt{\kappa}}{z^2(\tau')+1}\right) \\ -\left(\frac{1}{\sqrt{z^2(\tau)+1}} + i\lambda \frac{z(\tau)}{2(z^2(\tau)+1)^{\frac{3}{2}}}\right) \exp\left(-\int_{\tau_i}^{\tau} d\tau' \frac{\lambda\sqrt{\kappa}}{z^2(\tau')+1}\right) \\ -\left(\frac{1}{\sqrt{z^2(\tau)+1}} - i\lambda \frac{z(\tau)}{2(z^2(\tau)+1)^{\frac{3}{2}}}\right) \exp\left(-\int_{\tau_i}^{\tau} d\tau' \frac{\lambda\sqrt{\kappa}}{z^2(\tau')+1}\right) \\ 1 + \frac{z(\tau)}{\sqrt{z^2(\tau)+1}} \exp\left(-\int_{\tau_i}^{\tau} d\tau' \frac{\lambda\sqrt{\kappa}}{z^2(\tau')+1}\right) \end{pmatrix}. \end{aligned}$$

The normalization and Hermiticity conditions of the density matrix are verified. Thus, the state at the final time is determined by substituting $\tau_i \sim -\infty$, $\tau_f \sim \infty$, result-

ing in

$$|\rho(\tau_f)\rangle\rangle \sim \begin{pmatrix} \frac{1}{2}(1 - \exp(-4\pi\lambda\kappa)) \\ 0 \\ 0 \\ \frac{1}{2}(1 + \exp(-4\pi\lambda\kappa)) \end{pmatrix}.$$

Therefore, under the adiabatic approximation, $\rho(\tau_f)_{11}$ is given by

$$\rho_{11}(\tau_f) \sim \frac{1}{2} (1 - \exp(-4\pi\lambda\kappa)).$$

Appendix E: The comparisons with the Kayanuma formula

We first compute the transition probability in the regime where κ is sufficiently large ($\lambda\kappa \gg 1$). Next, we verify the defect density within the transverse-field Ising model under the condition of large κ . Our approximate solutions of the transition probability and the defect density are compared with those derived from the Kayanuma formula, which is effective in large λ .

First, we verify the behavior of the transition probability in the regime where κ is sufficiently large. the approximate solution Eq. (11) approaches $\frac{1}{2}$ as $\kappa \rightarrow \infty$, similar to the Kayanuma formula [30]

$$\langle \overline{P(\tau_f)} \rangle \sim p^{\text{Kayanuma}}(\kappa) = \frac{1}{2} (1 - \exp(-4\pi\kappa)).$$

The comparison between p^{Kayanuma} and $p^{\text{non-ad}} + p^{\text{ad}}$ is shown in Fig. 9. In the regime where κ is large, all cases asymptotically approach 1/2. However, since we are considering regions where λ is small, the p^{Kayanuma} failed to reproduce the behavior of the numerical results.

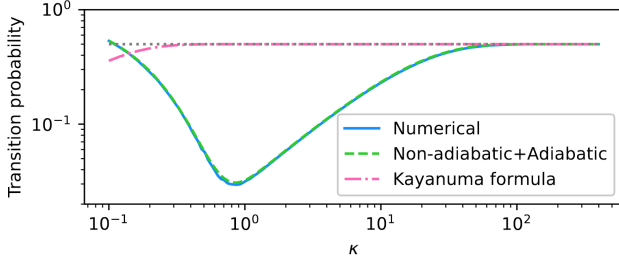


FIG. 9. Plots of the transition probabilities at τ_f against κ . The blue line (Numerical) represents the numerical simulation of Eq. (6) over the time span from $\tau_i = -200$ to $\tau_f = 200$. The green dashed line (Non-adiabatic+Adiabatic) represents $p^{\text{non-ad}} + p^{\text{ad}}$, while the red dashed line (Kayanuma formula) represents p^{Kayanuma} , with $\lambda = 10^{-3}$. The gray dashed line represents 1/2.

Next, We verify the defect density. The approximate solutions of Eq. (17) and Eq. (18) break down in the region where κ is large. In previous research [13], the following scaling for n in the regime of sufficiently large κ was proposed.

$$n^{\text{Kayanuma}}(\kappa) \sim \frac{1}{2} - \frac{1}{4\pi\sqrt{\kappa}}$$

On the other hand, by employing the asymptotic formulas of the functions $I_0(z)$ and $L_0(z)$, the expression can be reduced to the following by neglecting $\mathcal{O}(4\pi\lambda\kappa)^{-2}$

$$n^{\text{reciprocal}}(\lambda, \kappa) \sim n^{\text{KZM}}(\kappa) + \frac{1}{2} - \frac{1}{4\pi^2\lambda\kappa}.$$

We were able to confirm through Fig. 10 that this scaling yields the closer result to the numerical one than that of Kayanuma formula.

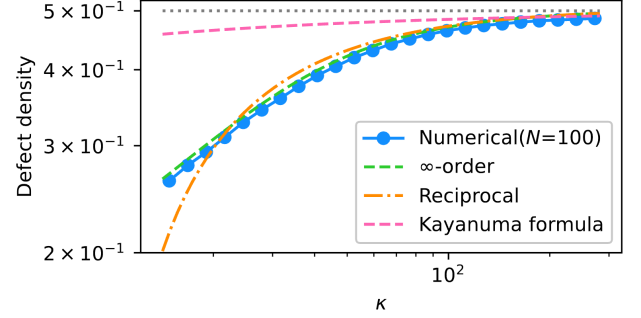


FIG. 10. Plots of the defect density against κ , focusing around $\kappa \gg 1$. The blue solid line (Numerical) represents the numerical simulation of Eq. (6) over the time span $\tau_i = -200$ to $\tau_f = 200$, plotting the discrete sum in Eq. (14), with $N = 100$. The green dashed line (∞ -order) represents $n^{\infty\text{-order}}$, the yellow dashed line (Reciprocal) represents $n^{\text{reciprocal}}$, and the pink dashed line (Kayanuma) represents n^{Kayanuma} , with $\lambda = 5 \times 10^{-3}$. The gray dot line represents 1/2.

-
- [1] W. H. Zurek, U. Dorner, and P. Zoller, *Phys. Rev. Lett.* **95**, 105701 (2005).
 - [2] B. Damski, *Phys. Rev. Lett.* **95**, 035701 (2005).
 - [3] J. Dziarmaga, *Phys. Rev. Lett.* **95**, 245701 (2005).
 - [4] A. Polkovnikov, *Phys. Rev. B* **72**, 161201 (2005).
 - [5] T. W. Kibble, *J. Phys. A: Math. Gen.* **9**, 1387 (1976).
 - [6] T. W. Kibble, *Phys. Rep.* **67**, 183 (1980).
 - [7] W. H. Zurek, *Nature* **317**, 505 (1985).
 - [8] W. H. Zurek, *Acta Phys. Pol. B* **24**, 1301 (1993).
 - [9] W. H. Zurek, *Phys. Rep.* **276**, 177 (1996).
 - [10] V. Mukherjee, U. Divakaran, A. Dutta, and D. Sen, *Phys. Rev. B* **76**, 174303 (2007).
 - [11] S. M. Griffin, M. Lilienblum, K. T. Delaney, Y. Kumagai, M. Fiebig, and N. A. Spaldin, *Phys. Rev. X* **2**, 041022 (2012).
 - [12] Z.-P. Gao, D.-W. Zhang, Y. Yu, and S.-L. Zhu, *Phys.*

- Rev. B **95**, 224303 (2017).
- [13] A. Dutta, A. Rahmani, and A. Del Campo, *Phys. rev. lett.* **117**, 080402 (2016).
- [14] M. Singh and S. Gangadharaiah, *Phys. Rev. B* **104**, 064313 (2021).
- [15] R. Puebla, A. Smirne, S. F. Huelga, and M. B. Plenio, *Phys. Rev. Lett.* **124**, 230602 (2020).
- [16] A. Polkovnikov, K. Sengupta, A. Silva, and M. Vengalattore, *Rev. Mod. Phys.* **83**, 863 (2011).
- [17] J.-M. Cui, Y.-F. Huang, Z. Wang, D.-Y. Cao, J. Wang, W.-M. Lv, L. Luo, A. Del Campo, Y.-J. Han, C.-F. Li, *et al.*, *Sci. rep.* **6**, 33381 (2016).
- [18] M.-Z. Ai, J.-M. Cui, R. He, Z.-H. Qian, X.-X. Gao, Y.-F. Huang, C.-F. Li, and G.-C. Guo, *Phys. Rev. A* **103**, 012608 (2021).
- [19] L. Wang, C. Zhou, T. Tu, H.-W. Jiang, G.-P. Guo, and G.-C. Guo, *Phys. Rev. A* **89**, 022337 (2014).
- [20] M. Gong, X. Wen, G. Sun, D.-W. Zhang, D. Lan, Y. Zhou, Y. Fan, Y. Liu, X. Tan, H. Yu, *et al.*, *Sci. Rep.* **6**, 22667 (2016).
- [21] S. Ulm, J. Roßnagel, G. Jacob, C. Degünther, S. Dawkins, U. Poschinger, R. Nigmatullin, A. Retzker, M. Plenio, F. Schmidt-Kaler, *et al.*, *Nat. commun.* **4**, 2290 (2013).
- [22] L. W. Clark, L. Feng, and C. Chin, *Science* **354**, 606 (2016).
- [23] D. Chen, M. White, C. Borries, and B. DeMarco, *Phys. Rev. Lett.* **106**, 235304 (2011).
- [24] K. Pyka, J. Keller, H. Partner, R. Nigmatullin, T. Burgermeister, D. Meier, K. Kuhlmann, A. Retzker, M. B. Plenio, W. Zurek, *et al.*, *Nat. commun.* **4**, 2291 (2013).
- [25] A. Del Campo, T. Kibble, and W. Zurek, *J. Phys. Condens. Matter* **25**, 404210 (2013).
- [26] S. Braun, M. Friesdorf, S. S. Hodgman, M. Schreiber, J. P. Ronzheimer, A. Riera, M. Del Rey, I. Bloch, J. Eisert, and U. Schneider, *Proc. Natl. Acad. Sci. USA* **112**, 3641 (2015).
- [27] M. Anquez, B. Robbins, H. Bharath, M. Boguslawski, T. Hoang, and M. Chapman, *Phys. rev. lett.* **116**, 155301 (2016).
- [28] H. Pichler, J. Schachenmayer, A. J. Daley, and P. Zoller, *Phys. Rev. A* **87**, 033606 (2013).
- [29] A. Rahmani, *Phys. Rev. A* **92**, 042110 (2015).
- [30] Y. Kayanuma, *J. Phys. Soc. Jpn.* **53**, 108 (1984).
- [31] M. Kenmoe, H. Phien, M. Kiselev, and L. Fai, *Phys. Rev. B* **87**, 224301 (2013).
- [32] B. Dóra, M. Heyl, and R. Moessner, *Nat. commun.* **10**, 2254 (2019).
- [33] B. Gulácsi and B. Dóra, *Phys. Rev. B* **103**, 205153 (2021).
- [34] V. Mukherjee and A. Dutta, *J. Stat. Mech. Theory Exp.* **2009**, P05005 (2009).
- [35] K. Mullen, E. Ben-Jacob, Y. Gefen, and Z. Schuss, *Phys. rev. lett.* **62**, 2543 (1989).
- [36] Y. Kayanuma and Y. Mizumoto, *Phys. Rev. A* **62**, 061401 (2000).
- [37] T. Suzuki and K. Iwamura, *Phys. Rev. B* **108**, 014110 (2023).
- [38] D. Patane, A. Silva, L. Amico, R. Fazio, and G. E. Santoro, *Phys. rev. lett.* **101**, 175701 (2008).
- [39] D. Patane, L. Amico, A. Silva, R. Fazio, and G. E. Santoro, *Phys. Rev. B* **80**, 024302 (2009).
- [40] S. Yin, P. Mai, and F. Zhong, *Phys. Rev. B* **89**, 094108 (2014).
- [41] P. Nalbach, S. Vishveshwara, and A. A. Clerk, *Phys. Rev. B* **92**, 014306 (2015).
- [42] D. Nigro, D. Rossini, and E. Vicari, *Phys. Rev. A* **100**, 052108 (2019).
- [43] D. Rossini and E. Vicari, *Phys. Rev. B* **100**, 174303 (2019).
- [44] D. Rossini and E. Vicari, *Phys. Rev. Res.* **2**, 023211 (2020).
- [45] E. A. Novikov, *Sov. Phys. JETP* **20**, 1290 (1965).
- [46] M. Sarandy and D. Lidar, *Phys. Rev. A* **71**, 012331 (2005).
- [47] I. S. Gradshteyn and I. M. Ryzhik, *Table of integrals, series, and products* (Academic press, 2014).
- [48] W. Heisenberg and H. Euler, *Z. Phys.* **98**, 714 (1936).
- [49] V. Weisskopf, *Mat. Fys. Medd.* **14**, 6 (1936).
- [50] J. Schwinger, *Phys. Rev.* **82**, 664 (1951).
- [51] R. Schützhold, H. Gies, and G. Dunne, *Phys. Rev. Lett.* **101**, 130404 (2008).
- [52] R. Nasri, *Integral Transforms Spec. Funct.* **27**, 181 (2016).